Characterization of direct Purkinje cell outputs to the brainstem

Christopher H. Chen[1,2,3,4], Zhiyi Yao[1,2,3], Shuting Wu[1], Wade G. Regehr[1,4]

[1]Department of Neurobiology, Harvard Medical School, Boston, MA, USA

[2]Department of Neural and Behavioral Sciences, The Pennsylvania State University, Hershey, Pennsylvania

[3]These authors contributed equally

[4]For correspondence: wade_regehr@hms.harvard.edu or chc5230@psu.edu

Abstract

Purkinje cells (PCs) primarily project to cerebellar nuclei but also directly innervate the brainstem. Some PC-brainstem projections have been described previously, but most have not been thoroughly characterized. Here we use a PC-specific cre line to anatomically and electrophysiologically characterize PC projections to the brainstem. PC synapses are surprisingly widespread, with the highest densities found in the vestibular and parabrachial nuclei. However, there are pronounced regional differences in synaptic densities within both the vestibular and parabrachial nuclei. Large optogenetically-evoked PC-IPSCs are preferentially observed in subregions with the highest densities of PC synapses, suggesting that PCs selectively influence these areas and the behaviors they regulate. Unexpectedly, the pontine central gray and nearby subnuclei also contained a low density of PC synapses, and large PC-IPSCs are observed in a small fraction of cells. We combined electrophysiological recordings with immunohistochemistry to assess the molecular identities of two putative PC targets: PC synapses onto mesencephalic trigeminal neurons were not observed even though these cells are in close proximity to PC boutons. PC synapses onto locus coeruleus neurons are exceedingly rare or absent, even though previous studies concluded that PCs are a major input to these neurons. The availability of a highly selective cre line for PCs allowed us to study functional synapses, while avoiding complications that can accompany the use of viral approaches. We conclude that PCs directly innervate numerous brainstem nuclei, but only inhibit a small fraction of cells in many nuclei. This suggests that PCs target cell types with specific behavioral roles in brainstem regions.

Introduction

Delineating the PC output pathways that mediate signals from the cerebellar cortex to the rest of the brain is a vital step in understanding cerebellar function. Although most studies of PC outputs have focused on the prominent connections to cerebellar nuclei [1,2], PCs also project directly to the brainstem. Extensive PC projections to vestibular nuclei [3-6] play vital roles in vestibular and ocular-related functions [7-9]. PCs also project to the prepositus hypoglossal nucleus, and this pathway may play a role in gaze stabilization [10-13]. In addition, PCs prominently project to the parabrachial nucleus, which is suited to regulate broad-ranging nonmotor and autonomic functions [14-18].

Several studies suggested that PCs also inhibit cells in other brainstem nuclei that could allow the cerebellum to control diverse behaviors. Rabies-based tracing approaches suggested that PCs are the primary inhibitory inputs to the locus coeruleus (LC) [19-21], but this is controversial. These studies have been highly influential and raised the possibility that PCs directly modulate LC-norepinephrine release, and regulate stress, attention, motivation, arousal, pain modulation, reward processing and other behaviors [22-27]. Furthermore, it was also suggested that disruption of the PC-LC pathway contributes to ASD and ADHD [28], and impairs the ability of the cerebellum to control seizures [29]. However, other studies do not see strong evidence for this PC-LC connection. Retrograde tracing studies of projections to the LC using dye tracers observed minimal PC labelling [30-32], and PC axons largely avoid the LC [17]. Thus, there is no consensus on whether PCs strongly inhibit LC neurons. There is also suggestive evidence that the cerebellum influences additional brainstem nuclei: the injection of trans-synaptic viruses into the posterior vermis labelled cells in pontine central grey (PCG) and nearby nuclei including the LC, Barrington's nucleus, dorsal tegmentum, and others [17]. These findings raise the possibility that direct PC projections could allow the cerebellum to regulate arousal, sleep-state transitions, micturition, and other behaviors [33-37]. However, the viruses used in these studies can also retrogradely label cells [38,39], and it is therefore necessary to assess whether there are functional PC synapses in these nuclei.

In this study, we determine whether PC make synapses and inhibit cells within various brainstem nuclei by determining whether PC synaptic boutons are present, and if PCs make functional synapses. Using *PCP2-cre/Ai34D (PC/synaptophysin-tdTomato)* mice to label PC synapses and map their locations, we find that PCs project widely in the brainstem, and that synaptic densities are highly nonuniform within different nuclei and subnuclei. We identify and characterize PC synapses in brainstem nuclei using optogenetics and *PCP2-cre/Ai32 (PC/ChR2-YFP)* mice. There was good agreement between the density of PC synaptic boutons and the probability of evoking PC-IPSCs in neurons within different regions and subregions. In regions with a low density of PC boutons, PC-IPSCs were typically observed in a small fraction of cells, raising the possibility that PCs selectively target specific types of neurons in these regions. These findings provide an important resource that will allow future studies to clarify the PC targets in various brainstem nuclei and the behaviors controlled by these output pathways.

Results

Visualization of PC projections to the brainstem

We visualized PC synapses in the brainstem of *PC/synaptophysin-tdTomato* mice in which synaptic boutons are intensely labelled, and axons, dendrites and somata weakly labelled. We imaged

synaptophysin-tdTomato in both sagittal (**Fig. 1A**) and coronal sections (**Fig. 1B**), and aligned the images to the Allen Common Coordinate Framework (CCF) [40] based on the contours of the tissue. We collapsed the vestibular subnuclei (MV, LAV etc.) into the VN, and labelled the territories encompassing the dorsomedial pons as simply the PCG (see **Methods**). Likewise, the rostral/caudal or medial/lateral divisions of other nuclei are not annotated specifically (PGRN, NTS, etc.).

In low magnification images (**Fig. 1A, 1B,** *left images*), labeling is observed in the cerebellar nuclei and brainstem. In sagittal views, brainstem labeling is sparser in the medial sections than in lateral sections. In coronal sections, the brainstem labeling is densest at bregma -5.85 mm, and sparser in anterior and posterior sections. Medium (**Fig. 1A, 1B,** *2nd column from left*) and high magnification images (**Fig. 1A, 1B i-iv**) showed highly variable densities of PC boutons in different regions. In some regions, labelling was extremely faint for medium magnification images, but PC synapses were apparent at higher magnifications (for example, in the PCG in **Fig. 1Aa i** and **Fig. 1Ba ii**).

There were pronounced regional differences in the extent of labelling within the VN and the PB. In sagittal sections, for the VN the densest PC labelling was observed ventral to the cerebellar nuclei and the fourth ventricle (**Fig. 1Ac ii**), and expression fanned out ventrally, anteriorly, and posteriorly. Dense labeling of the VN was also present in the anterior dorsal regions of the other sagittal slices (**Fig. 1Aa ii, Fig. 1Ab ii+iii, Fig. 1Ac ii, Fig. 1Ad ii**). Although PC boutons were present throughout the VN, in anterior regions the densities were low near the midline (**Fig. 1Aa iii, Fig. 1Ab iv**) and moderate densities in more lateral sections (**Fig. 1Ac iv, Fig. 1Ad iv**). The density gradient of PC synapses within the VN was more apparent in coronal sections. Synaptic densities were highest in dorsal VN (**Fig. 1Bb i+ii, Fig. 1Bc i, Fig. 1Bd i, Fig. 1Be ii**), and lower in ventral VN (**Fig. 1Ba iii, Fig. 1Bb iii, Fig. 1Bc iii, Fig. 1Bd ii**). A gradient of labelling was also apparent within the PB. The highest densities were present in posterior PB (**Fig. 1Ac i**, **Fig. 1Ba i**). The differences in the densities of PC synapses within subregions of the VN and the PB suggest that PCs preferentially regulate specific subregions.

Low levels of labelling were apparent in many other brainstem regions. In the PCG, fluorescence is apparent in high magnification views (**Fig. 1Aa i**, **Fig. 1Ba ii+iv)**. Sparse labelling is present in the PRP (**Fig. 1Ba-d iv**), which is consistent with previous studies [10-13]. Very little labelling was found in the GRN (**Fig. 1Aa iv**), the PRNr (**Fig. 1Ad iii**), the LC (**Fig. 1Ab i**), and the NTS (**Fig. 1Be iii**).

These fluorescence images establish that there is considerable variation in the densities of PC synapses between and within various brainstem regions. The highest densities of PC synapses are present in the range bregma -5.85 mm to -5.95 mm, and 1.5 to 2 mm from the midline. Notably PC synapses were only observed in the dorsal region of the brainstem.

Quantification of PC synapses in the brainstem

To quantify the densities of PC synapses in the brainstem, we detected individual PC boutons, and registered images to the Allen CCF. Experiments were performed in *CGRP-GFP/PCP2-cre/synaptophysin-tdTomato* mice. We used synaptophysin-tdTomato fluorescence to label PC synapses, vGAT immunohistochemistry to visualize all GABAergic synapses, and CGRP-GFP to label subnuclei to aid in atlas alignment. The resulting alignment is shown for a coronal slice (**Fig. 2A,** see **Methods**). To quantify synapses, confocal images were taken for a z-stack of 1.5 µm of the dorsal brainstem bilaterally. All regions previously observed with tdTomato signal **(Fig 1)** were imaged, as well as additional sections with no obvious labeling within 100 µm of labelled regions. Since weak tdTomato labeling is observed in the axons of PCs, vGAT immunohistochemistry was used to help identify

putative pre-synaptic sites. In addition, PC contributions to total inhibition in each region can be measured by comparing GABAergic boutons (**Fig. 2B,** *lower right, grey dots*) with or without tdTomato colabelling (**Fig. 2B,** *lower right, red dots,* see **Methods**). This approach identifies putative presynaptic sites but does not identify functional synapses.

This approach was used to detect putative PC boutons in a series of coronal slices from Bregma -5.45 to -6.95, where the majority of PC projections reside. Inhibitory synapses were present at high densities in all regions in all slices (**Fig. 2C**, *left, grey*), while PC synapses were spatially restricted (**Fig. 2C**, *left, red*). The total number of detected PC boutons, the density of PC synapses, and the fraction of inhibitory boutons that are made by PCs, were determined for each region (**Fig. 2D-F**, data points color-coded to indicate slice position, n = 3 mice, 2 hemispheres/mouse). Areas with observable PC boutons were selected for display along with their near neighbors, including example areas with no tdTomato labeling (PGRNd, SPVI, NTSl, NTSm). Areas ventral to displayed regions were not labelled.

High densities of PC synapses are present in the superior, lateral, spinal and medial vestibular nuclei, but there are pronounced regional differences in bouton densities within the subnuclei and related nuclei (**Fig. 2C-F**). In the superior vestibular nucleus, PC synapses are present at high density and comprise up to 85% of all inhibitory inputs. In the lateral vestibular nucleus, the number, density, and fractional contribution of PC synapses, were largest in posterior sections. PC inputs contributed to ~40% of all inhibitory inputs in posterior LAV. The medial vestibular nucleus spanned the longest anterior-posteriorly and has the most PC synapses in the middle sections, from bregma -6.05 mm to -6.35 mm. There was a pronounced dorsal-ventral gradient in the density of PC synapses. The spinal vestibular nucleus is the most posterior nucleus and had less variability across the anterior-posterior axis. It has a high average PC synapse number and density across sections and 26% of inhibition originates from PCs. The prepositus nucleus also receives PC inputs that are highest at bregma -6.05 mm and -6.35 mm and highest in dorsal regions. PCs contribute up to 9% of the total inhibitory inputs in the prepositus nucleus (**Fig. 2D** *left, middle, right*). In the more posterior sections (bregma -6.65 mm and -6.95 mm), PC synapses were restricted to the dorsal region in the vestibular nuclei, the external cuneate, and the cuneate. The external cuneate and the cuneate are small regions, and the densities were correspondingly higher though the absolute number of synapses are relatively low and variable. The external cuneate spanned from bregma -6.65mm to -6.95 but has more PC synapses in the posterior section. It is evident that the vestibular nuclei, the cuneate nucleus and prepositus nucleus are not uniformly targeted by PCs.

There is a posterior to anterior gradient of PC synapses in the PB. In anterior sections (**Fig. 2C**, bregma -5.45 mm to -5.65 mm) high densities of PC synapses were only apparent in a few localized regions of the PB. The medial-ventral region of the PB (bregma -5.65 mm) has extensive PC inputs, comparable in density to some regions of the vestibular nuclei.

PC synapses are present but at low densities within the pontine central gray (PCG) and nearby subnuclei including the LC, Barrington's nucleus, sublateraldorsal nucleus, lateraldorsal tegmenta nucleus, dorsal tegmental nucleus, and supragenual nucleus (**Fig. 2C**, bregma -5.45 mm to -5.65 mm). PC synapses make up a small fraction of inhibitory synapses in these areas (**Fig. 2F**). The Barrington's nucleus and the laterodorsal tegmental nucleus had a higher PC density and fraction of inhibition, although it is important to note that these PCG subregions are relatively small in area. The LC, which is labelled in CGRP mice, had few PC synapses with a slightly elevated PC density count in a few posterior sections.

Characterization of functional properties of PC synapses in the brainstem

To confirm these PC connections in different brainstem regions and examine their strength, we optically stimulated PC fibers in *PC/ChR2-YFP* mice and measured IPSCs in coronal brain slices of the dorsal brainstem. It is likely that this approach provides a good estimate of connectivity even when PC axons are cut, because severed axons expressing ChR2 can be optogenetically activated to evoke synaptic responses[41-44]. We recorded optically-evoked IPSCs in 133 of 310 neurons in the dorsal brainstem (between bregma -5.45 mm to -6.35 mm) to generate a physiological map of PC inputs to the brainstem. The IPSC amplitudes of the recorded brainstem neurons (**Fig 3A**, greyscale color-coded) are shown along with the density maps of PC boutons from **Fig 2**. For the density map, PC bouton counts were binned into 144 x 144 x 4 µm volumes, and averaged across the multiple sections. The likelihood of optically-evoking a PC-IPSC varied with coronal section from anterior to posterior was 9%, 32%, 51%, and 45% (-5.45, -5.65, -6.05 and -6.35 mm to Bregma). We quantified the response amplitudes (**Fig. 3B**), probability of evoking a PC-IPSC (**Fig. 3C**), and the IPSC amplitudes (**Fig. 3D**).

In the most anterior slices (Bregma -5.45 mm and -5.65 mm), PC-IPSCs were not evoked at most locations (47/53 cells nonresponding), which is consistent with the very low density of PC synaptic boutons (**Fig. 3A**). For the PCG, no PC-IPSCs were evoked in the Bregma -5.45 mm section. In the Bregma -5.65 mm section PC-IPSCs were evoked in 23% of cells, with highly variable amplitudes (**Fig. 3B**), and the average PC-IPSC in responding cells was over 1 nA (**Fig. 3D**). For the PB, PC-IPSCs were evoked with a low response probability in Bregma -5.45 mm slices, but at Bregma -5.65 mm, 48% of cells responded (**Fig. 3C**). In the PB, the amplitudes of IPSCs onto different cells were highly variable (50 pA to over 10 nA) (**Fig. 3B)**, and the average of responding cells was 2 nA.

In more posterior slices (Bregma -6.05 mm and -6.35), PC-IPSCs were evoked in a high percentage of cells in the SUV, LAV, MV, and PRP (45%, 59%, 58%, and 52% respectively**, Fig. 3C**). The SUV and LAV had predominantly large IPSCs in responding cells, with most evoked currents larger than 500 pA and the average PC-IPSC of responding cells was several nanoamps. In the SPIV, MV, and PRP, PC-IPSCs ranged from 50 pA to ~2nA and average IPSC amplitudes of responding cells was less than 1 nA (**Fig. 3B, D**). Overall, PC-IPSCs were evoked in a larger percentage of cells in regions with a high density of PC boutons (**Fig. 3E**).

Assessing PC inputs to the LC and mesencephalic trigeminal neurons

There are many types of molecularly distinct neurons in the brainstem [45], which could be differentially targeted by PCs and contribute to the highly heterogeneous amplitudes of evoked PC-IPSCs we observed. We therefore took a targeted approach to record from neurons in the MEV and LC, which are distinct neuron populations with well-characterized markers that are in close proximity to PC boutons and to areas with large PC inputs (the PB and vestibular nuclei, **Fig 4A**). Previous trans-synaptic tracing efforts had also suggested potential PC inputs to these cells, but functional characterizations of these connections are lacking [17,19-21].

We began by studying the extremely large unipolar neurons of the MEV. These neurons are developmentally part of the periphery, gap junction coupled, exhibit a unique chloride gradient, and directly sense and control the muscles of the jaw [46-48]. We used immunohistochemistry for parvalbumin (PV) to identify MEV neurons [47]. We measured PC-IPSCs, filled cells with biocytin, and identified these neurons based on their shape and PV expression (**Fig. 4B**). Recordings were made in both coronal slices (bregma -5.45 mm and -5.65 mm) and horizontal slices, but PC-IPSCs were not evoked in any of

the recorded cells (**Fig. 4C,** n=23). Thus, despite their close proximity to PC synapses, PCs do not provide a significant source of inhibition to MEV neurons.

We also used optogenetics and immunohistochemistry to examine PC-IPSCs in the LC to directly assess whether PCs provide a major source of inhibition to LC neurons, as has been proposed [19-21]. The low density of PC synapses in the LC raised doubts about whether PCs provide a prominent source of inhibition in the LC (**Fig. 4A**), but it was possible that PCs might synapse onto LC dendrites that extend beyond the core of the LC. We therefore directly assessed PC-LC synaptic connectivity by measuring optically-evoked PC-IPSCs using a recording electrode containing biocytin, and used immunohistochemistry to identify TH-expressing neurons of the LC (**Fig. 4B**). We examined the LC at two coronal levels in the posterior LC and found that no PC-IPSCs were evoked in the anterior section (0/27), while small currents were evoked in 2/40 neurons in posterior sections (bregma -5.65 mm) **(Fig. 4C, D)**. The average PC-IPSC of all cells was 1.4 ± 8.2 pA, Thus, PCs do not provide a prominent source of inhibition to the LC.

Discussion

Widespread but nonuniform PC inputs to the brainstem

Here we find that PCs make direct synapses within numerous brainstem nuclei. The densities of these synapses vary widely in different nuclei. There is also a pronounced gradient of PC synapses across the dorsal-ventral axis of the several brainstem nuclei, indicating that PCs do not uniformly regulate activity within these nuclei. The combination of synaptophysin-TdT expression restricted to PCs and vGAT immunohistochemistry allowed us to quantify the absolute number and density of PC synapses, and the fraction of inhibitory inputs that are from PCs for each region. PC synapses comprised up to 75% of the inhibitory synapses in some vestibular regions and 55% in the caudal PB. Thus, PCs make prominent contributions to inhibition in some brainstem regions that are comparable to levels observed in cerebellar nuclei (72%) [49]. In contrast, in the PRP and PCG PCs provide a low total number of inputs (PRP, PCG, vs. VN; 0.002, 0.006, >0.01 synapses/μm^2 respectively) and a small fraction of inhibitory inputs (4, 8%, 15-50%), where they inhibit only a modest fraction of cells (13%, 33%, 54%). In all of these regions, PCs likely function similarly to their inputs to the cerebellar nuclei, where a very brief pause in firing can lead to large and rapid elevations in target cell firing [50,51], but PCs regulate the firing of a very different fraction of cells in brainstem nuclei and can do so in a variety of different ways[5,52,53].

PC synapses in the PCG and nearby regions

We establish that there are PC boutons within the PCG and associated nuclei, and that there are strong PC synapses in this region. This suggests that PCs play a role in regulating activity in these regions and in the behaviors they control. However, the PCG is enigmatic in structure and function, with the most commonly used mouse atlases disagreeing on the borders and identity of subnuclei [40,54,55] (see Methods). Barrington's nucleus, a region that controls micturition [36,37], stands out as being well defined anatomically and functionally, and is a promising candidate for regulation by PCs. Our previous study raised the possibility that PCs in the posterior vermis might directly target cells in Barrington's nucleus [17], but this study relied on AAV1 injections in the cerebellum, that in addition to anterogradely labelling PC targets, could have retrogradely labeled cells in Barrington's nucleus if they project to the cerebellar

cortex. Our results highlight the challenges in studying PC synapses in the PCG and related nuclei. We observed PC synapses and synaptic connections for cells in the vicinity of Barrington's nucleus (**Fig. 2** and **Fig. 3**). As suggestive as these findings are, it remains an open question whether direct PC synapses to Barrington's nucleus control micturition without additional experiments using molecular markers to identify Barrington's nucleus. Similarly, further studies are needed to identify other PC targets in the PCG and determine what behaviors they control.

Gradients of PC synapses in the brainstem

In general, PCs inputs to brainstem nuclei are spatially heterogenous. The caudal-rostral gradient of PC synapses in the PB allows PCs to target specific subtypes of PB neurons [17]. We find that PC synapses in the PCG and nearby subnuclei also exhibit a caudal-rostral gradient. Additional studies are needed to identify PC targets in these regions and to determine the significance of their spatial heterogeneity. There is also a pronounced dorsal-ventral gradient in many vestibular subnuclei and related nuclei. Previous studies suggested that PCs do not project to all regions of the VN, but they were unable to quantify the regional densities of PC synapses. Labeling individual PCs or those within subregions of the cerebellar cortex helped to determine their specific projections in the VN [3,16,56-58], but did not label all PC synapses in the VN. Immunohistochemical methods targeting proteins selectively expressed in PCs offer the potential to label all PC synapses in the VN. Calbindin is a widely used PC marker, but its presence in vestibular afferents compromises its use in the VN [59]. PKCγ is also expressed by PCs, but has the advantage that it is not present in vestibular afferents [4]. The lack of PKCγ immunoreactivity established that PC synapses are absent in the ventral VN, which is qualitatively similar to what we observe. However, the possibility that PKCγ is expressed by other cell types projecting to the VN complicates the use of PKCγ labeling as a definitive marker for identifying PC synapses. Our studies establish that PC synapses are present at high densities throughout the SUV; in the dorsal LAV, MV, PRP, SPIV; in subregions of the ECU; and there are large subregions that are devoid of PC synapses. Multiple lines of evidence suggest that PC synapses in the VN play a role in cancelling self-motion related to eye movements and proprioception [10]. The distribution of synapses suggests that processing within VN subnuclei is spatially segregated according to the locations of PC synapses, implying that PC feedback potentially cancels signals related to self-motion specifically within these regions.

Brainstem regulation by direct PC inputs or indirectly via the deep cerebellar nuclei

PCs can also disynaptically influence the brainstem by disinhibiting cells in the deep cerebellar nuclei that in turn project to the brainstem. It is likely that some brainstem regions receive both direct PC input and indirect from deep cerebellar nuclei [22,60,61], and that these two different pathways serve different roles. For example, direct and indirect inputs target different regions of the PB are implicated in different behaviors [17,62]. The deep cerebellar nuclei projections to the vestibular nuclei are not well understood, but they are likely a mix of excitatory and inhibitory inputs [60,61,63].This raises the possibility that the indirect pathway through the deep cerebellar nuclei has the added flexibility of providing both excitation and inhibition.

Lack of significant PC inputs to LC neurons

We find that PCs do not provide a significant direct input to the LC. This has been controversial because retrograde labelling studies using rabies viruses concluded that PCs constitute one of the largest groups of cells projecting to the LC [19](Fig 2h,i), even though PC synapses did not appear to innervate the core of the LC ([17] and **Fig. 1**, **Fig. 2**). We directly assessed PC to LC connection

strengths using a cre line that is highly selective for PCs, and we found that in *PC/ChR2-YFP* mice, tiny optically-evoked PC-IPSCs (~50 pA) were observed in just 3% of LC neurons. The average IPSC size for all cells was less than 2 pA. This indicates that within the LC, inhibition originates from brain regions other than PCs [21]. The cerebellum may still regulate firing in the LC, but it does so via connections through the deep cerebellar nuclei and the LC [24,30,31].

Together, these findings indicate that reliance on anatomical tracing experiments alone is insufficient to establish the presence and importance of a synaptic connection. Studies highlighting PC inputs to the LC were conducted using rabies-tracing methods [19-21], which have limitations. These viruses have unknown tropism, unclear synapse specificity, and critically depend on the degree to which the "starter" cell population is restricted to the intended cell type, which can be complicated by inappropriate expression, and by the sensitivity of TVA-based rabies infection[64,65]. We were fortunate to have a highly selective cre line to selectively target PCs that allowed us to examine PC synapses in the brainstem while avoiding complications that can occur when using viruses.

PC targets in the brainstem

The next step in clarifying the PC to brainstem outputs and the behaviors they regulate is to determine the molecular identity of target cells. This is challenging because there are many types of neurons present in the brainstem [45,66-68]. We previously identified candidate PC targets by injecting AAV1 in the cerebellar cortex to anterogradely label PC targets, and then using RNA-seq to determine the molecular identity of labelled cells [17]. An important caveat to this approach is that it while it very effectively labels anterograde PC targets, it can also retrogradely label cells that project to the cerebellar cortex. It is therefore crucial to determine if functional PC synapse are present, unless it is known that the region does not project to the cerebellar cortex.

Our primary focus in our previous study [17] was to identify PC targets in the PB. The fact that the PB does not project to the posterior vermis of the cerebellum [69,70], and the observation that labelled cells were restricted to PB regions receiving PC inputs, suggest that the following cells are PC targets: *Satb2*, *Penk*, and *Tacr1* populations, which have roles in taste [71,72], thermoregulation [73], and pain [74,75], respectively. We also found that CGRP neurons [70,76,77], which are located in a region of the PB devoid of PC synapses, were not labelled by this method. This supports the hypothesis that PCs selectively inhibit specific types of brainstem neurons.

We also labelled neurons in the vestibular nucleus, Barrington's nucleus, mesencephalic trigeminal nucleus, and the locus coeruleus in that previous study. The lack of PC-evoked inputs to neurons in the mesencephalic trigeminal nucleus and locus coeruleus shown here established that these populations are not targeted by PCs. It further suggests that these neurons project to the cerebellum and were retrogradely labelled[78,79]. For the multiple candidate PC targets in the vestibular nucleus, it is necessary to specifically test for the presence of PC synapses, as was done for floccular-targeting, *GlyT2* expressing neurons [5,6]. In the PCG and nearby nuclei, the sparsity of PC synapses combined with the large PC synaptic inputs in a small fraction of cells suggests that PCs only inhibit specific cells in these regions. This was also reflected in our previous anatomical experiments[17], where we identified *Crh*-expressing Barrington's neurons and other glutamatergic/GABAergic neurons in the PCG. These cells are important for micturition [36] and valence [33] respectively, and further indicate a broad range of PC output functions.

Methods

Animals

For anatomical studies, B6.Cg-Tg(PCP2-cre)3555Jdhu/J x B6;129S-Gt(ROSA)26Sor$^{tm34.1(CAG-Syp/tdTomato)Hze}$/J (*PC/synaptophysin-tdTomato*, Jackson Labs) was used. Calca-GFP (*CGRP-GFP*) (MMRRC, Stock number: 011187-UCD, generously provided by David Ginty) mice were crossed with the *PC/synaptophysin-tdTomato* mice to further support anatomical studies. For physiology experiments, B6.Cg-Tg(PCP2-cre)3555Jdhu/J × B6;129S-Gt(ROSA)26Sor$^{tm32(CAG-COP4*H134R/EYFP)Hze}$/J (*PC/ChR2-YFP*, Jackson Laboratory) mice were used. All animals were used under supervision of Harvard Medical School's Institutional Animal Care and Use Committee (IACUC) or the Pennsylvania State University College of Medicine's IACUC.

Anatomy

In order to identify inhibitory synapses PCs made in the brainstem, *PC/synaptophysin-tdTomato* mice were crossed with CGRP-GFP mice. Thus, synaptophysin-tdTomato was expressed selectively in all PCs and GFP is expressed in the lateral parabrachial nuclei, the LC, the hypoglossal nuclei, the vestibular nerve, the spinal tract of the trigeminal nerve, and the solitary tracts. Mice were anesthetized at P56 and perfused with PBS and 4% PFA. After removal, brains were post-fixed for one day in 4% PFA, and sliced coronally and sagittally in 50 µm sections. Slices were stained with a vGAT (vesicular GABA transporter) antibody (Synaptic Systems, #131 004, 1:500), and visualized using an AlexaFluor 647 secondary (Thermo Fisher, #A-21450, 1:1000). Every third section of the dorsal brainstem was imaged on a confocal microscope (Leica Stellaris 5). Acquisitions were made with an XY resolution of 361.1 nm for an area of about 10 mm^2 total per section, and 300 nm z steps for 4 µm stacks. Stitched images were imported into ZEISS arivis Pro (arivis).

To identify PC synapses, we analyzed for synaptophysin-tdTomato fluorescence colabeled with vGAT fluorescence[17,80]. Using a background correction feature in arivis, a background representation was generated with a 50 µm diameter Gaussian filter and subtracted from the vGAT fluorescence. vGAT was then isolated by a watershed algorithm provided with a 1 µm bouton diameter and threshold intensity. Thresholds were adjusted for each individual image based on three 50-pixel squares that had various densities of vGAT expression. Optimal threshold values were approximately one standard deviation above median. The following analysis were conducted in MATLAB: segmented vGAT boutons were analyzed for tdTomato-synaptophysin colocalization by finding a regional maximum in the tdTomato fluorescence (maximum center-to-center distance is 0.7 µm). We plotted the synaptophysin intensity values within each voxel. This histogram showed a bimodal distribution corresponding to noise and signal, and the signal threshold corresponded to the minimum between the two peaks.

We identified brainstem nuclei by aligning the Allen Common Coordinate Framework. We used several features to register confocal images of the brainstem: 1) the edges of the tissue and position of the ventricles, 2) the fiber tracts and features notable from autofluorescence and brightfield imaging, and 3) GFP labelling present in numerous brainstem regions in CGRP-GFP mice (including VIIn, sptv, LC, XII, and their axons). CGRP-GFP labelling in the LC and VIIn was particularly useful in anterior sections.

Puncta within each brainstem region were quantified using this aligned atlas. We matched our samples to the indicated bregma levels (±100 µm) in **Figure 2**. To determine the variability in our alignment, we sampled 50-70 points 350 µm apart across the atlas image before and after aligning to each confocal

image. The displacement distances of these reference points were calculated for each image and binned based on the confocal image location relative to bregma. Our images were displaced from the Allen Common Coordinate Framework by an average of 107 µm. The displacement distances were 90 ± 25 µm (standard deviation, n=6 hemispheres, bregma -5.45 mm), 126±26 µm (n=10, bregma -5.65 mm),102±35 µm (n=8, bregma -6.05 mm),103±51 µm (n=8, bregma -6.35 mm). 108±43 µm (n=8, bregma -6.65 mm), 96±31 µm (n=8, bregma -6.95 mm).

It is important to note that the accuracy of our mapping is dependent on the accuracy of the reference maps that we register to. The PCG is one region in particular that varies substantially between reference atlases [40,54,55]. We labelled the regions in/around the dorsomedial pons as the PCG, based off of the borders noted in the Allen CCF, but other atlases constrain the borders of the PCG, leaving parts of the dorsomedial pons effectively unlabelled. The precise location of many other regions within the dorsomedial pons also differ dramatically. Precise identification of these areas (i.e. Barrington's nucleus) will require a molecularly targeted approach (*in situ hybridization*, etc.).

Electrophysiology

Mice of both sexes ranging from p24 to p50 (n=30) were anesthetized with ketamine / xylazine and transcardially perfused with warm choline ACSF solution (34°C) containing in mM: 110 Choline Cl, 2.5 KCl, 1.25 NaH_2PO_4, 25 $NaHCO_3$, 25 glucose, 0.5 $CaCl_2$, 7 $MgCl_2$, 3.1 Na Pyruvate, 11.6 Na ascorbate, 0.002 (R,S)-CPP, 0.005 NBQX, oxygenated with 95% O_2 / 5% CO_2. Coronal slices were made (200 µm) using a Leica 1200S or a Campden Instrument 7000smz-2 vibratome in warm choline ACSF (34°C). Slices were then transferred to a holding chamber with warm ACSF (34°C) containing in mM: 127 NaCl, 2.5 KCl, 1.25 NaH_2PO_4, 25 $NaHCO_3$, 25 glucose, 1.5 $CaCl_2$, 1 $MgCl_2$ and were recovered at 34°C for 30 minutes before being moved to room temperature until recordings began.

Voltage-clamp recordings were made across the brainstem. Borosilicate glass electrodes (2-4 MΩ) were filled with a high chloride internal containing in mM: 35 CsF, 100 CsCl, 10 EGTA, 10 HEPES, 4 QX-314, pH 7.3 with CsOH. This internal solution was used to increase sensitivity to inhibitory inputs and improve clamp. The osmolarity of internal solution was adjusted to 290-300 mOsm. Whole-cell capacitance and series resistance was left uncompensated for all experiments. Neurons were held at -70 mV. All experiments were performed at room temperature in the presence of 5 µM NBQX to block AMPARs and 2.5 µM (R,S)-CPP to block NMDARs, with a flow rate of 2 ml/min. ChR2 expressing PC axons were stimulated with 473 nm light from a light-emitting diode (Thorlabs or Sutter) in the entire field of view (1 ms, ~80 mW/mm^2) for at least 10 trials. Data were collected using Igor (Wavemetrics) running mafPC (courtesy of M. A. Xu-Friedman) or SutterPatch (Sutter). Images with a 4X objective were used to determine the positions of recorded cells. Slices were fixed and stained with DAPI to confirm the anterior-posterior position of the coronal slice, and matched to the closest indicated bregma level indicated in **Figure 3**.

In experiments targeting the LC or mesencephalic trigeminal nucleus, biocytin (B1592, Thermofisher) was included in the intracellular solution. Cells were then stained with an anti-tyrosine hydroxylase antibody to identify the LC (1:1000, AB152, Sigma) or anti-parvalbumin antibody to identify the mesencephalic trigeminal (1:1000 P3088, Sigma), followed by an Alexa 647 secondary antibody (1:1000 A32733 or ab150079, Thermofisher or Abcam respectively) and streptavidin-Alexa 594 conjugate (1:1000, 1402-3900, Thermofisher). Sections were subsequently imaged using a confocal microscope (Leica Stellaris 5) to determine the identity of the recorded cell.

Acknowledgements

This work was supported by grants from the National Institutes of Health: R01NS032405 and R35NS097284 to W.G.R., R00NS110978 to C.H.C., and NINDS P30 Core Center (NS072030) to the Neurobiology Imaging Center at Harvard Medical School. Shuting Wu was supported by the Lefler Center at Harvard Medical School.

References

1 Kebschull, J. M. *et al.* Cerebellum Lecture: the Cerebellar Nuclei-Core of the Cerebellum. *Cerebellum* **23**, 620-677, doi:10.1007/s12311-022-01506-0 (2024).
2 Hull, C. & Regehr, W. G. The Cerebellar Cortex. *Annu Rev Neurosci* **45**, 151-175, doi:10.1146/annurev-neuro-091421-125115 (2022).
3 Barmack, N. H. Central vestibular system: vestibular nuclei and posterior cerebellum. *Brain Res Bull* **60**, 511-541, doi:10.1016/s0361-9230(03)00055-8 (2003).
4 Barmack, N. H., Qian, Z. & Yoshimura, J. Regional and cellular distribution of protein kinase C in rat cerebellar Purkinje cells. *J Comp Neurol* **427**, 235-254, doi:10.1002/1096-9861(20001113)427:2<235::aid-cne6>3.0.co;2-6 (2000).
5 Shin, M. *et al.* Multiple types of cerebellar target neurons and their circuitry in the vestibulo-ocular reflex. *J Neurosci* **31**, 10776-10786, doi:10.1523/JNEUROSCI.0768-11.2011 (2011).
6 Sekirnjak, C., Vissel, B., Bollinger, J., Faulstich, M. & du Lac, S. Purkinje cell synapses target physiologically unique brainstem neurons. *J Neurosci* **23**, 6392-6398, doi:10.1523/JNEUROSCI.23-15-06392.2003 (2003).
7 Lisberger, S. G. & Pavelko, T. A. Brain stem neurons in modified pathways for motor learning in the primate vestibulo-ocular reflex. *Science* **242**, 771-773, doi:10.1126/science.3142040 (1988).
8 Lisberger, S. G., Pavelko, T. A. & Broussard, D. M. Responses during eye movements of brain stem neurons that receive monosynaptic inhibition from the flocculus and ventral paraflocculus in monkeys. *J Neurophysiol* **72**, 909-927, doi:10.1152/jn.1994.72.2.909 (1994).
9 Lisberger, S. G., Pavelko, T. A. & Broussard, D. M. Neural basis for motor learning in the vestibuloocular reflex of primates. I. Changes in the responses of brain stem neurons. *J Neurophysiol* **72**, 928-953, doi:10.1152/jn.1994.72.2.928 (1994).
10 Cullen, K. E. Internal models of self-motion: neural computations by the vestibular cerebellum. *Trends Neurosci* **46**, 986-1002, doi:10.1016/j.tins.2023.08.009 (2023).
11 Graham, J. A. *et al.* Angular Head Velocity Cells within Brainstem Nuclei Projecting to the Head Direction Circuit. *J Neurosci* **43**, 8403-8424, doi:10.1523/JNEUROSCI.0581-23.2023 (2023).
12 Walberg, F. & Dietrichs, E. The interconnection between the vestibular nuclei and the nodulus: a study of reciprocity. *Brain Res* **449**, 47-53, doi:10.1016/0006-8993(88)91022-0 (1988).
13 Voogd, J., Gerrits, N. M. & Ruigrok, T. J. Organization of the vestibulocerebellum. *Ann N Y Acad Sci* **781**, 553-579, doi:10.1111/j.1749-6632.1996.tb15728.x (1996).
14 Sugihara, I. *et al.* Projection of reconstructed single Purkinje cell axons in relation to the cortical and nuclear aldolase C compartments of the rat cerebellum. *J Comp Neurol* **512**, 282-304, doi:10.1002/cne.21889 (2009).
15 De Zeeuw, C. I., Wylie, D. R., DiGiorgi, P. L. & Simpson, J. I. Projections of individual Purkinje cells of identified zones in the flocculus to the vestibular and cerebellar nuclei in the rabbit. *J Comp Neurol* **349**, 428-447, doi:10.1002/cne.903490308 (1994).
16 Wylie, D. R., De Zeeuw, C. I., DiGiorgi, P. L. & Simpson, J. I. Projections of individual Purkinje cells of identified zones in the ventral nodulus to the vestibular and cerebellar nuclei in the rabbit. *J Comp Neurol* **349**, 448-463, doi:10.1002/cne.903490309 (1994).

17 Chen, C. H. *et al.* A Purkinje cell to parabrachial nucleus pathway enables broad cerebellar influence over the forebrain. *Nat Neurosci* **26**, 1929-1941, doi:10.1038/s41593-023-01462-w (2023).
18 Hashimoto, M. *et al.* Anatomical Evidence for a Direct Projection from Purkinje Cells in the Mouse Cerebellar Vermis to Medial Parabrachial Nucleus. *Front Neural Circuits* **12**, 6, doi:10.3389/fncir.2018.00006 (2018).
19 Schwarz, L. A. *et al.* Viral-genetic tracing of the input-output organization of a central noradrenaline circuit. *Nature* **524**, 88-92, doi:10.1038/nature14600 (2015).
20 Sun, P. *et al.* Sex-Related Differential Whole-Brain Input Atlas of Locus Coeruleus Noradrenaline Neurons. *Front Neural Circuits* **14**, 53, doi:10.3389/fncir.2020.00053 (2020).
21 Breton-Provencher, V. & Sur, M. Active control of arousal by a locus coeruleus GABAergic circuit. *Nat Neurosci* **22**, 218-228, doi:10.1038/s41593-018-0305-z (2019).
22 Novello, M., Bosman, L. W. J. & De Zeeuw, C. I. A Systematic Review of Direct Outputs from the Cerebellum to the Brainstem and Diencephalon in Mammals. *Cerebellum* **23**, 210-239, doi:10.1007/s12311-022-01499-w (2024).
23 Kang, S. *et al.* Recent Advances in the Understanding of Specific Efferent Pathways Emerging From the Cerebellum. *Front Neuroanat* **15**, 759948, doi:10.3389/fnana.2021.759948 (2021).
24 Carlson, E. S. *et al.* Catecholaminergic Innervation of the Lateral Nucleus of the Cerebellum Modulates Cognitive Behaviors. *J Neurosci* **41**, 3512-3530, doi:10.1523/JNEUROSCI.2406-20.2021 (2021).
25 Zeidler, Z., Hoffmann, K. & Krook-Magnuson, E. HippoBellum: Acute Cerebellar Modulation Alters Hippocampal Dynamics and Function. *J Neurosci* **40**, 6910-6926, doi:10.1523/JNEUROSCI.0763-20.2020 (2020).
26 Froula, J. M., Hastings, S. D. & Krook-Magnuson, E. The little brain and the seahorse: Cerebellar-hippocampal interactions. *Front Syst Neurosci* **17**, 1158492, doi:10.3389/fnsys.2023.1158492 (2023).
27 Krohn, F. *et al.* The integrated brain network that controls respiration. *Elife* **12**, doi:10.7554/eLife.83654 (2023).
28 Koevoet, D., Deschamps, P. K. H. & Kenemans, J. L. Catecholaminergic and cholinergic neuromodulation in autism spectrum disorder: A comparison to attention-deficit hyperactivity disorder. *Front Neurosci* **16**, 1078586, doi:10.3389/fnins.2022.1078586 (2022).
29 Streng, M. L. & Krook-Magnuson, E. The cerebellum and epilepsy. *Epilepsy Behav* **121**, 106909, doi:10.1016/j.yebeh.2020.106909 (2021).
30 Cedarbaum, J. M. & Aghajanian, G. K. Afferent projections to the rat locus coeruleus as determined by a retrograde tracing technique. *J Comp Neurol* **178**, 1-16, doi:10.1002/cne.901780102 (1978).
31 Aston-Jones, G., Ennis, M., Pieribone, V. A., Nickell, W. T. & Shipley, M. T. The brain nucleus locus coeruleus: restricted afferent control of a broad efferent network. *Science* **234**, 734-737, doi:10.1126/science.3775363 (1986).
32 Aston-Jones, G. & Waterhouse, B. Locus coeruleus: From global projection system to adaptive regulation of behavior. *Brain Res* **1645**, 75-78, doi:10.1016/j.brainres.2016.03.001 (2016).
33 Xiao, C. *et al.* Glutamatergic and GABAergic neurons in pontine central gray mediate opposing valence-specific behaviors through a global network. *Neuron* **111**, 1486-1503 e1487, doi:10.1016/j.neuron.2023.02.012 (2023).
34 Park, S. H. & Weber, F. Neural and Homeostatic Regulation of REM Sleep. *Front Psychol* **11**, 1662, doi:10.3389/fpsyg.2020.01662 (2020).
35 Keller, J. A. *et al.* Voluntary urination control by brainstem neurons that relax the urethral sphincter. *Nat Neurosci* **21**, 1229-1238, doi:10.1038/s41593-018-0204-3 (2018).
36 Hou, X. H. *et al.* Central Control Circuit for Context-Dependent Micturition. *Cell* **167**, 73-86 e12, doi:10.1016/j.cell.2016.08.073 (2016).

37 Verstegen, A. M. J., Vanderhorst, V., Gray, P. A., Zeidel, M. L. & Geerling, J. C. Barrington's nucleus: Neuroanatomic landscape of the mouse "pontine micturition center". *J Comp Neurol* **525**, 2287-2309, doi:10.1002/cne.24215 (2017).
38 Zingg, B. *et al.* AAV-Mediated Anterograde Transsynaptic Tagging: Mapping Corticocollicular Input-Defined Neural Pathways for Defense Behaviors. *Neuron* **93**, 33-47, doi:10.1016/j.neuron.2016.11.045 (2017).
39 Zingg, B., Peng, B., Huang, J., Tao, H. W. & Zhang, L. I. Synaptic Specificity and Application of Anterograde Transsynaptic AAV for Probing Neural Circuitry. *J Neurosci* **40**, 3250-3267, doi:10.1523/JNEUROSCI.2158-19.2020 (2020).
40 Wang, Q. *et al.* The Allen Mouse Brain Common Coordinate Framework: A 3D Reference Atlas. *Cell* **181**, 936-953 e920, doi:10.1016/j.cell.2020.04.007 (2020).
41 Mao, T. *et al.* Long-range neuronal circuits underlying the interaction between sensory and motor cortex. *Neuron* **72**, 111-123, doi:10.1016/j.neuron.2011.07.029 (2011).
42 Petreanu, L., Huber, D., Sobczyk, A. & Svoboda, K. Channelrhodopsin-2-assisted circuit mapping of long-range callosal projections. *Nat Neurosci* **10**, 663-668, doi:10.1038/nn1891 (2007).
43 Petreanu, L., Mao, T., Sternson, S. M. & Svoboda, K. The subcellular organization of neocortical excitatory connections. *Nature* **457**, 1142-1145, doi:10.1038/nature07709 (2009).
44 Jackman, S. L., Beneduce, B. M., Drew, I. R. & Regehr, W. G. Achieving high-frequency optical control of synaptic transmission. *J Neurosci* **34**, 7704-7714, doi:10.1523/JNEUROSCI.4694-13.2014 (2014).
45 Nardone, S. *et al.* A spatially-resolved transcriptional atlas of the murine dorsal pons at single-cell resolution. *Nat Commun* **15**, 1966, doi:10.1038/s41467-024-45907-7 (2024).
46 Curti, S., Hoge, G., Nagy, J. I. & Pereda, A. E. Synergy between electrical coupling and membrane properties promotes strong synchronization of neurons of the mesencephalic trigeminal nucleus. *J Neurosci* **32**, 4341-4359, doi:10.1523/JNEUROSCI.6216-11.2012 (2012).
47 Florez-Paz, D., Bali, K. K., Kuner, R. & Gomis, A. A critical role for Piezo2 channels in the mechanotransduction of mouse proprioceptive neurons. *Sci Rep* **6**, 25923, doi:10.1038/srep25923 (2016).
48 Yokomizo, Y. *et al.* Excitatory GABAergic synaptic potentials in the mesencephalic trigeminal nucleus of adult rat in vitro. *Neurosci Res* **51**, 463-474, doi:10.1016/j.neures.2004.12.016 (2005).
49 De Zeeuw, C. I. & Berrebi, A. S. Postsynaptic targets of Purkinje cell terminals in the cerebellar and vestibular nuclei of the rat. *Eur J Neurosci* **7**, 2322-2333, doi:10.1111/j.1460-9568.1995.tb00653.x (1995).
50 Han, K. S., Chen, C. H., Khan, M. M., Guo, C. & Regehr, W. G. Climbing fiber synapses rapidly and transiently inhibit neighboring Purkinje cells via ephaptic coupling. *Nat Neurosci* **23**, 1399-1409, doi:10.1038/s41593-020-0701-z (2020).
51 Wu, S., Wardak, A., Khan, M. M., Chen, C. H. & Regehr, W. G. Implications of variable synaptic weights for rate and temporal coding of cerebellar outputs. *Elife* **13**, doi:10.7554/eLife.89095 (2024).
52 Najac, M. & Raman, I. M. Integration of Purkinje cell inhibition by cerebellar nucleo-olivary neurons. *J Neurosci* **35**, 544-549, doi:10.1523/JNEUROSCI.3583-14.2015 (2015).
53 Ozcan, O. O. *et al.* Differential Coding Strategies in Glutamatergic and GABAergic Neurons in the Medial Cerebellar Nucleus. *J Neurosci* **40**, 159-170, doi:10.1523/JNEUROSCI.0806-19.2019 (2020).
54 Paxinos, G. & Franklin, K. B. *Paxinos and Franklin's the mouse brain in stereotaxic coordinates*. (Academic press, 2019).
55 Kronman, F. A. *et al.* Developmental Mouse Brain Common Coordinate Framework. *bioRxiv*, doi:10.1101/2023.09.14.557789 (2023).

56 Shojaku, H., Sato, Y., Ikarashi, K. & Kawasaki, T. Topographical distribution of Purkinje cells in the uvula and the nodulus projecting to the vestibular nuclei in cats. *Brain Res* **416**, 100-112, doi:10.1016/0006-8993(87)91501-0 (1987).
57 Tabuchi, T., Umetani, T. & Yamadori, T. Corticonuclear and corticovestibular projections from the uvula in the albino rat: differential projections from sublobuli of the uvula. *Brain Res* **492**, 176-186, doi:10.1016/0006-8993(89)90900-1 (1989).
58 Blot, F. G. C. *et al.* Purkinje cell microzones mediate distinct kinematics of a single movement. *Nat Commun* **14**, 4358, doi:10.1038/s41467-023-40111-5 (2023).
59 Kevetter, G. A. Pattern of selected calcium-binding proteins in the vestibular nuclear complex of two rodent species. *J Comp Neurol* **365**, 575-584, doi:10.1002/(SICI)1096-9861(19960219)365:4<575::AID-CNE5>3.0.CO;2-1 (1996).
60 Fujita, H., Kodama, T. & du Lac, S. Modular output circuits of the fastigial nucleus for diverse motor and nonmotor functions of the cerebellar vermis. *Elife* **9**, doi:10.7554/eLife.58613 (2020).
61 Judd, E. N., Lewis, S. M. & Person, A. L. Diverse inhibitory projections from the cerebellar interposed nucleus. *Elife* **10**, doi:10.7554/eLife.66231 (2021).
62 Hwang, K. D. *et al.* Cerebellar nuclei neurons projecting to the lateral parabrachial nucleus modulate classical fear conditioning. *Cell Rep* **42**, 112291, doi:10.1016/j.celrep.2023.112291 (2023).
63 Bagnall, M. W. *et al.* Glycinergic projection neurons of the cerebellum. *J Neurosci* **29**, 10104-10110, doi:10.1523/JNEUROSCI.2087-09.2009 (2009).
64 Beier, K. T. The Serendipity of Viral Trans-Neuronal Specificity: More Than Meets the Eye. *Front Cell Neurosci* **15**, 720807, doi:10.3389/fncel.2021.720807 (2021).
65 Rogers, A. & Beier, K. T. Can transsynaptic viral strategies be used to reveal functional aspects of neural circuitry? *J Neurosci Methods* **348**, 109005, doi:10.1016/j.jneumeth.2020.109005 (2021).
66 Langlieb, J. *et al.* The molecular cytoarchitecture of the adult mouse brain. *Nature* **624**, 333-342, doi:10.1038/s41586-023-06818-7 (2023).
67 Zhang, M. *et al.* Molecularly defined and spatially resolved cell atlas of the whole mouse brain. *Nature* **624**, 343-354, doi:10.1038/s41586-023-06808-9 (2023).
68 Kodama, T. *et al.* Neuronal classification and marker gene identification via single-cell expression profiling of brainstem vestibular neurons subserving cerebellar learning. *J Neurosci* **32**, 7819-7831, doi:10.1523/JNEUROSCI.0543-12.2012 (2012).
69 Huang, D., Grady, F. S., Peltekian, L. & Geerling, J. C. Efferent projections of Vglut2, Foxp2, and Pdyn parabrachial neurons in mice. *J Comp Neurol* **529**, 657-693, doi:10.1002/cne.24975 (2021).
70 Huang, D., Grady, F. S., Peltekian, L., Laing, J. J. & Geerling, J. C. Efferent projections of CGRP/Calca-expressing parabrachial neurons in mice. *J Comp Neurol* **529**, 2911-2957, doi:10.1002/cne.25136 (2021).
71 Fu, O. *et al.* SatB2-Expressing Neurons in the Parabrachial Nucleus Encode Sweet Taste. *Cell Rep* **27**, 1650-1656 e1654, doi:10.1016/j.celrep.2019.04.040 (2019).
72 Jarvie, B. C., Chen, J. Y., King, H. O. & Palmiter, R. D. Satb2 neurons in the parabrachial nucleus mediate taste perception. *Nat Commun* **12**, 224, doi:10.1038/s41467-020-20100-8 (2021).
73 Norris, A. J., Shaker, J. R., Cone, A. L., Ndiokho, I. B. & Bruchas, M. R. Parabrachial opioidergic projections to preoptic hypothalamus mediate behavioral and physiological thermal defenses. *Elife* **10**, doi:10.7554/eLife.60779 (2021).
74 Barik, A. *et al.* A spinoparabrachial circuit defined by Tacr1 expression drives pain. *Elife* **10**, doi:10.7554/eLife.61135 (2021).
75 Deng, J. *et al.* The Parabrachial Nucleus Directly Channels Spinal Nociceptive Signals to the Intralaminar Thalamic Nuclei, but Not the Amygdala. *Neuron* **107**, 909-923 e906, doi:10.1016/j.neuron.2020.06.017 (2020).

76 Campos, C. A., Bowen, A. J., Roman, C. W. & Palmiter, R. D. Encoding of danger by parabrachial CGRP neurons. *Nature* **555**, 617-622, doi:10.1038/nature25511 (2018).

77 Palmiter, R. D. The Parabrachial Nucleus: CGRP Neurons Function as a General Alarm. *Trends Neurosci* **41**, 280-293, doi:10.1016/j.tins.2018.03.007 (2018).

78 Billig, I., Yatim, N., Compoint, C., Buisseret-Delmas, C. & Buisseret, P. Cerebellar afferences from the mesencephalic trigeminal nucleus in the rat. *Neuroreport* **6**, 2293-2296, doi:10.1097/00001756-199511270-00006 (1995).

79 Stanley, A. T., Post, M. R., Lacefield, C., Sulzer, D. & Miniaci, M. C. Norepinephrine release in the cerebellum contributes to aversive learning. *Nat Commun* **14**, 4852, doi:10.1038/s41467-023-40548-8 (2023).

80 Guo, C., Rudolph, S., Neuwirth, M. E. & Regehr, W. G. Purkinje cell outputs selectively inhibit a subset of unipolar brush cells in the input layer of the cerebellar cortex. *Elife* **10**, doi:10.7554/eLife.68802 (2021).

Table 1 Abbreviations of Brainstem Anatomical Regions

	Nuclei		
B	Barrington's Nucleus	PRP	Prepositus Nucleus
CU	Cuneate Nucleus	SG	Supragenual Nucleus
DCO	Dorsal Cochlear Nucleus	SLD	Sublaterodorsal Nucleus
DTN	Dorsal Tegmental Nucleus	SPIV	Spinal Vestibular Nucleus
ECU	External Cuneate Nucleus	SPVI	Spinal Nucleus of the Trigeminal
GRN	Gigantocellular Reticular Nucleus	SUT	Supratrigeminal Nucleus
IP	Interposed Nucleus	SUV	Superior Vestibular Nucleus
LAV	Lateral Vestibular Nucleus	VN	Vestibular Nucleus
LC	Locus Coeruleus	X	Nucleus X
LDT	Laterodorsal Tegmental Nucleus	XII	Hypoglossal Nucleus
MEV	Mesencephalic Trigeminal Nucleus	Y	Nucleus Y
MV	Medial Vestibular Nucleus		
NI	Nucleus Incertus		**Ventricles**
NTS	Nucleus of the Solitary Tract	V4	Fourth Ventricles
NTSl	Nucleus of the Solitary Tract, lateral	V4r	Fourth Ventricle (Lateral Recess)
NTSm	Nucleus of the Solitary Tract, medial		**Fiber Tracts**
PARN	Parvicellular Reticular Nucleus	arb	Arbor vitae
PB	Parabrachial Nuclei	icp	Inferior cerebellar peduncle
PCG	Pontine Central Gray	scp	Superior cerebellar peduncle
PGRN	Paragigantocellular Reticular Nucleus	sptv	Spinal tract of the trigeminal nerve
PGRNd	Paragigantocellular Reticular Nucleus, dorsal	VIIn	Facial nerve
PRNr	Pontine Reticular Nucleus	vVIIIn	Vestibular nerve

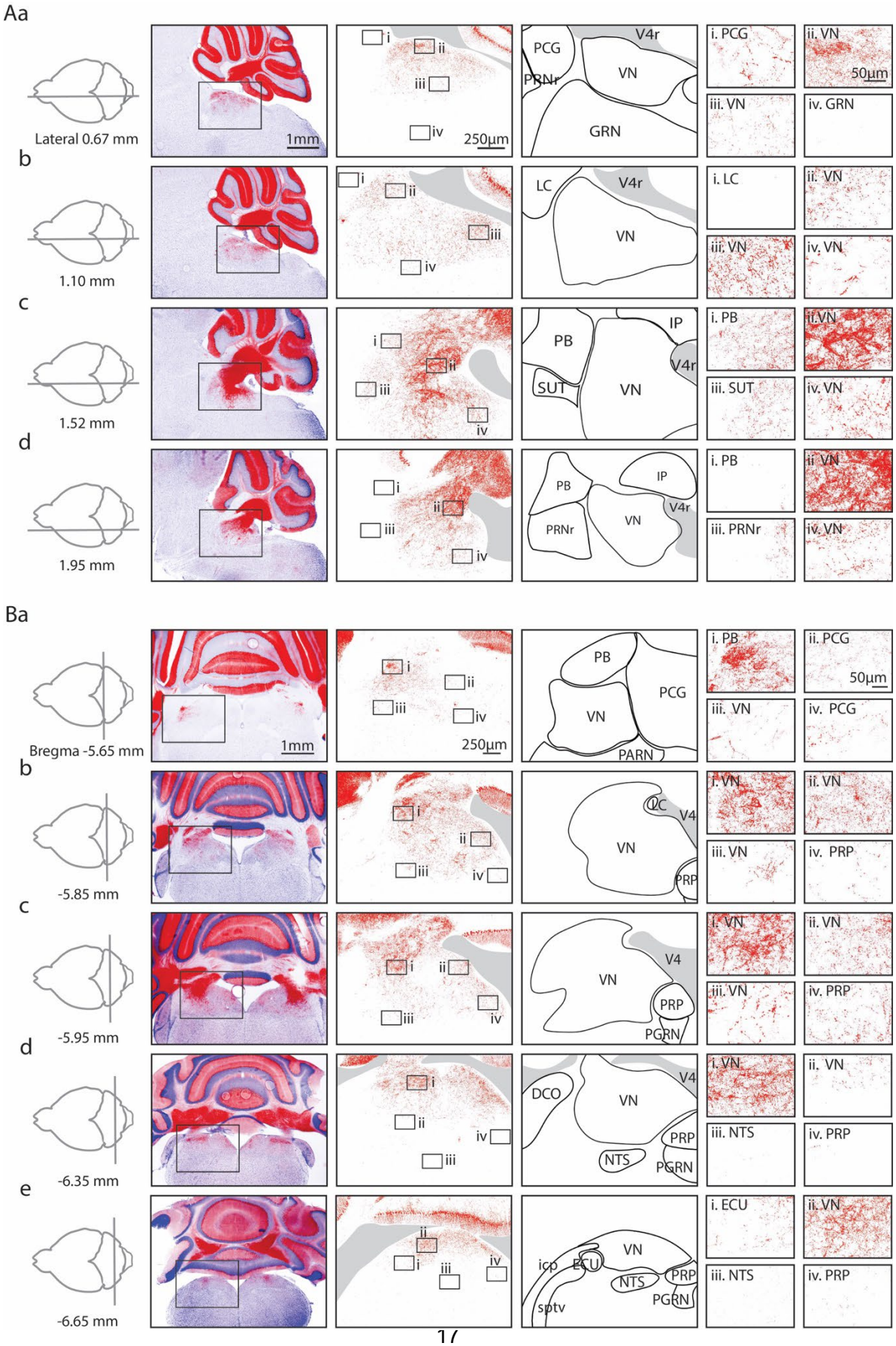

Figure 1: Anatomical characterization of Purkinje cell outputs to the brainstem using *PC/synaptophysin-tdTomato* mice.

Aa. *First column.* Diagram showing parasagittal slice location.

Second column. Low magnification views of tdTomato (tdT) fluorescence (red) in the cerebellar cortex and brainstem.

Third column. Medium magnification views of the regions indicated in Ab.

Fourth column. Anatomical regions corresponding to the preceding column.

Last column. i-iv. High magnification views of the regions indicated in the preceding column.

Ab-d. As in Aa, but for subsequent parasagittal slices.

B. As in A, but for coronal slices.

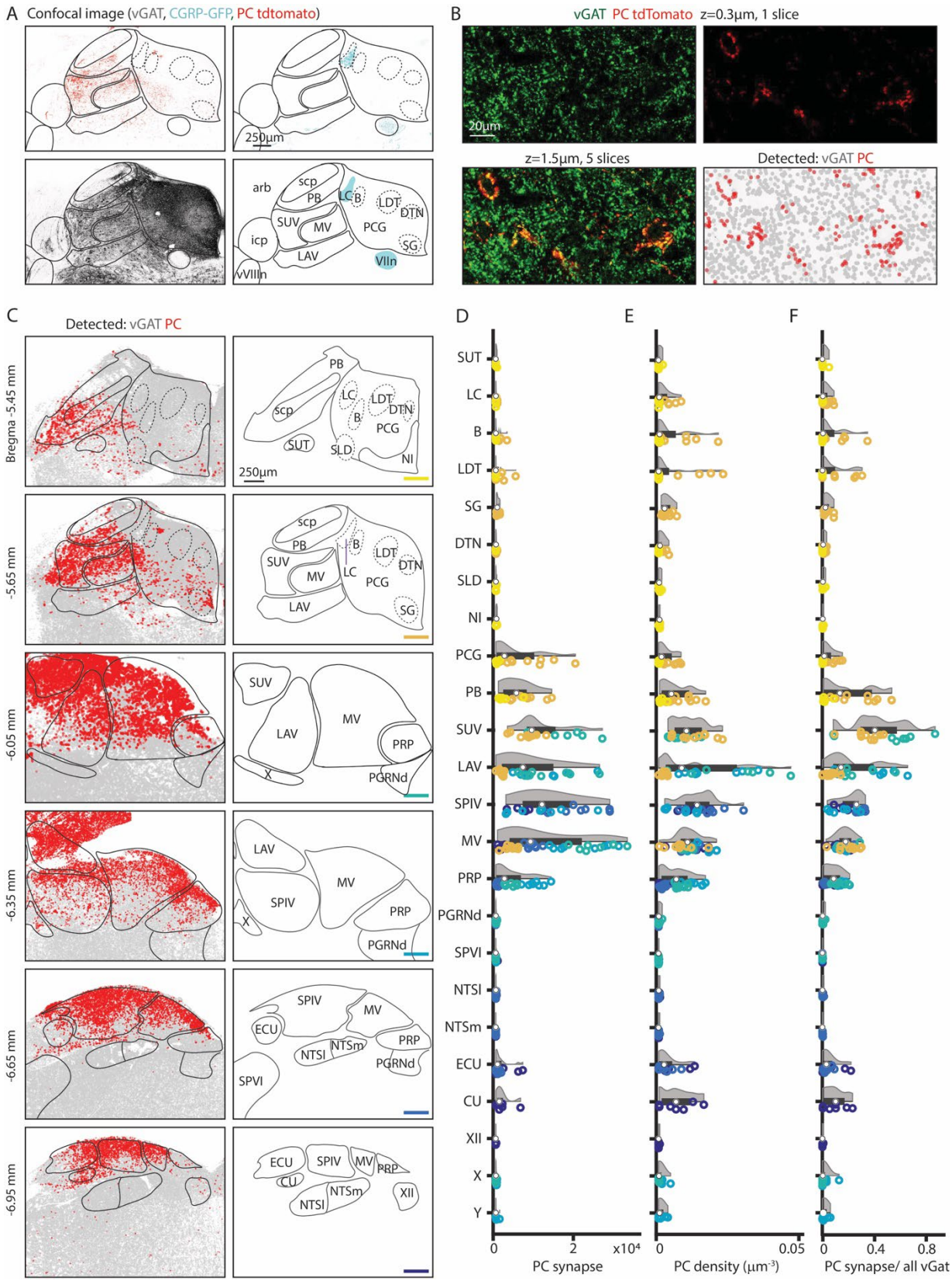

Figure 2: Quantification of Purkinje cell synapses in the brainstem. GABAergic boutons were detected using a vGAT antibody and PC presynaptic boutons were detected based on tdT-synaptophysin labelling in *PC/synaptophysin-tdTomato* mice.

A. (*upper left*) Confocal image of td-Tomato fluorescence.

(*upper right*) GFP fluorescence in CGRP-GFP mouse in which the locus coeruleus and facial nerve are labelled.

(*lower left*) vGAT labelling of GABAergic boutons.

(*lower right)* Allen Atlas coronal section corresponding to confocal images with landmarks used for registration highlighted in cyan.

B. (*upper left*) vGAT labelling in a single confocal section.

(*upper right*) tdT labelling in a single confocal section.

(*lower left*) z-stack of vGAT and tdT labelling in 5 sections (1.5 µm thick).

(*lower right*) Detected GABAergic boutons based on vGAT labelling (*grey*) and PC boutons (*red*).

C. (*left*) Detected GABAergic boutons corresponding to PCs (*red*), and neurons other than PCs (*grey*) from six example coronal sections.

(*right)* Labelled anatomic regions for each coronal section.

D. Number of PC synapses detected per section in each region. Individual section values are represented with symbol colors correspond to the sections in C, right (bottom right corner color bars). Violin plot of the region shown in grey with average and quartile values in black.

E. Density of PC boutons in each region. Individual section and region average as represented in D.

F. Percentages of GABAergic boutons that correspond to PCs for each region. Individual section and region average as represented in D.

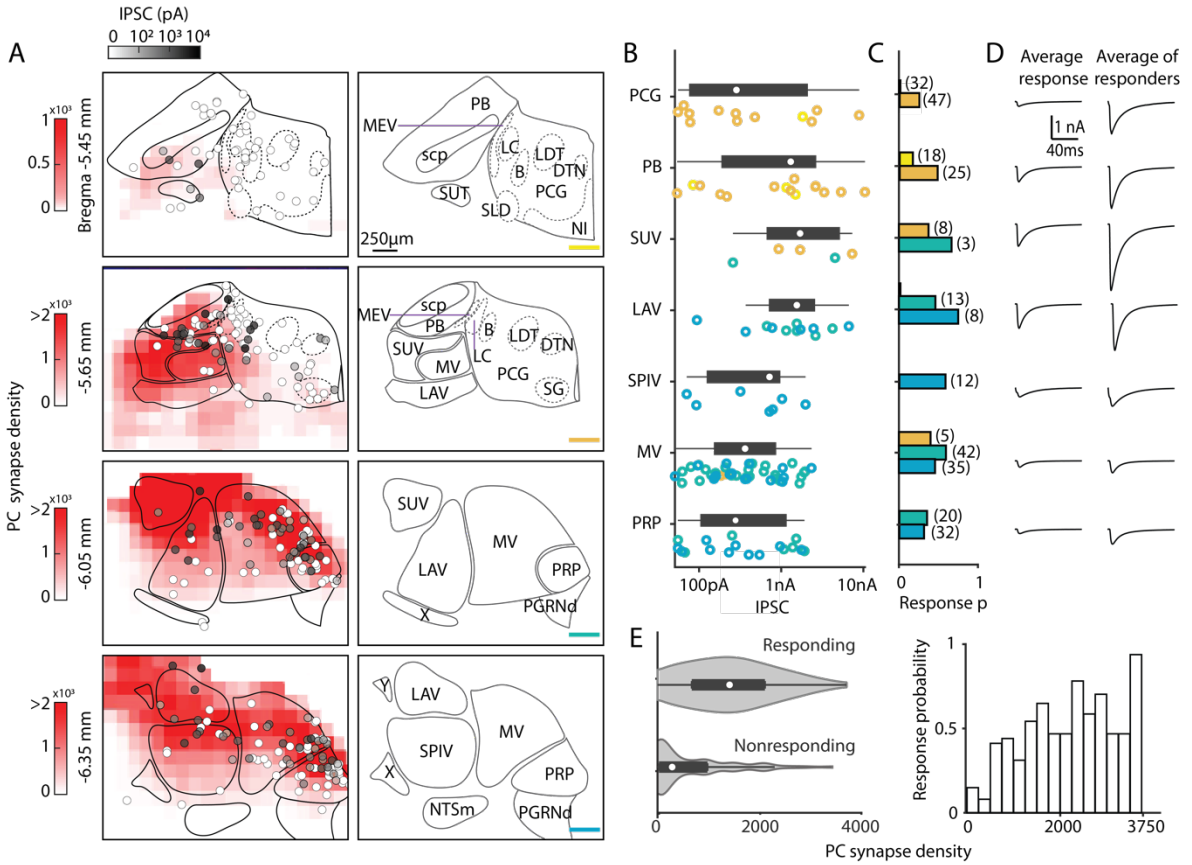

Figure 3. Characterization of functional properties of PC synapses in the brainstem. Light-evoked PC-IPSCs were measured in the brainstem of *PC/ChR2-YFP* mice.

A. (*left*) Averaged PC synapse density from previous quantification of brainstem regions (red, from **Figure 2**). Synapses were binned in voxels of 144x144x4 µm. The locations of all recorded neurons are shown with the symbols coded for the light-evoked IPSC amplitudes (n=310)

(*right*) Labeled anatomical regions are indicated and the position of each slice is color coded, as in **Figure 2**.

B. Evoked amplitudes of the responding neurons (n=113) in each region are shown. Symbol colors correspond to the sections in A.

C. Fraction of responding cells in each brainstem region and total number of neurons recorded (n=300). Bar graph colors correspond to the sections in A.

D. (*left*) Average current in each region for all cells.

(*right*) Average current of responding cells in each region.

E. (*left*) A violin plot of the average PC synapses densities for neurons where a light-evoked PC-IPSC was detected (responding) and for cells were such a response was not observed (nonresponding).

(*right*) The probability of observing a light-evoked PC-IPSC in neurons is plotted as a function of the density of PC synaptic boutons in that voxel.

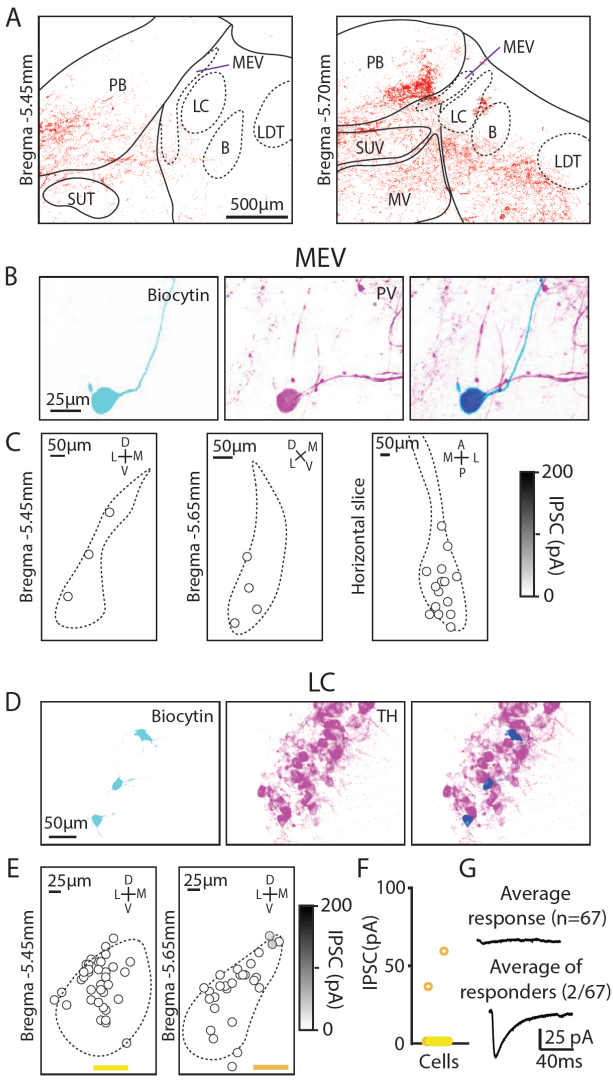

Figure 4 Minimal PC inputs to locus coeruleus and mesencephalic trigeminal neurons

A. Example confocal image of PC presynaptic boutons labeled by synaptophysin-tdT showing cases where labeling was near locus coeruleus and the mesencephalic trigeminal nuclei.

B. (*left*) Biocytin was included in the pipette to label MEV cells during whole-cell recordings.

(*middle*) MEV cells visualized with a PV antibody.

(*right*) Colocalization of biocytin and PV confirms that patched neurons were PV+ MEV neurons.

C. Locations of MEV cells in two coronal slices and one horizontal slice. No PC-IPSC responses were detected in any of the cells (n=23) at any location.

D. As in B, but for LC cells labelled with a TH antibody

E. As in C, but for two coronal levels of the LC (n=67).

F. Summary of the amplitudes of PC IPSCs recorded in LC cells.

G. Average PC-LC neuron IPSCs for all cells (n=65 *left*), and for cells where a synaptic response was detected (n=2, *right*).